Linking drought strategy to climate of origin in a widespread C4 grass: hydraulic traits, xylem anatomy and stomatal behaviour in *Themeda triandra*

Vinod Jacob, Chris J. Blackman, Brendan Choat, Brian J. Atwell, Eloise Foo, Alejandro Correa-Lozano, Travis Britton, Emma E. Sumner, Ian J. Wright

SUMMARY

- Hydraulic, stomatal and anatomical traits strongly influence drought survival and productivity, but the extent to which these trait-types are coordinated and relate to climate-of-origin in herbaceous species remains poorly understood.

- We quantified hydraulic, stomatal and anatomical traits in eight populations of *Themeda triandra* selected from diverse temperature and precipitation regimes across Australia, grown under common conditions and exposed to drought. Trait – climate-of-origin relationships were quantified using multiple linear mixed models.

- Leaf xylem embolism resistance (P_{50}) was unrelated to climate-of-origin precipitation. Instead, plants from drier climates exhibited lower maximum stomatal conductance, earlier stomatal closure during drought and higher stomatal safety margins (the difference between water potential at stomatal closure and P_{50}). Plants from warmer climates exhibited greater embolism resistance and higher hydraulic conductance, along with wider vessels and lower vein density, suggesting adaptation to high evaporative demand.

- Our findings highlight two primary hydraulic strategies related to climate-of-origin: 1) conservative water use and drought avoidance in drier climates, and 2) embolism resistance and hydraulic efficiency in warmer climates. These findings provide new insights into the intraspecific differences in traits and adaptive strategies used by C_4 grasses to persist in contrasting climates.

INTRODUCTION

Understanding the physiological and anatomical adaptations that underpin plant success in different environments is a primary goal of plant ecology and critical for predicting vegetation responses to climate change (Bjorkman *et al.*, 2018). Hydraulic traits, which govern how plants transport and retain water, play a central role in determining plant survival and productivity (Choat *et al.*, 2012). A key measure of how plants maintain function under water deficit is the water potential (-MPa) at which 50% of hydraulic conductivity is lost due to embolism, P_{50} (Choat *et al.*, 2018). While resistance to xylem embolism defines the lower bounds of water potential that a plant can tolerate before irreversible drought injury occurs, the likelihood of reaching this critical threshold is largely modulated by stomatal regulation (Skelton *et al.*, 2015, Martin-StPaul *et al.*, 2017). Stomata respond to soil water deficit through gradual closure, minimizing water loss and slowing further declines in xylem water potential. By comparing water potential thresholds of stomatal closure (e.g., 90% closure; g_{s90}) and P_{50}, a "stomatal safety margin" (SSM) can be defined where SSM = $P_{50} - g_{s90}$. Hydraulic strategies vary widely among plants, ranging from conservative (isohydric; stomata close in advance of xylem failure/high SSM) to risky (anisohydric; stomata remain open even after the onset of embolism/neutral or negative SSM) (Hochberg *et al.*, 2018; Hartmann *et al.*, 2021). In this study we examined variation in P_{50}, g_{s90} and SSM across populations of the widespread C4 grass, *T. triandra*, grown under common conditions. We tested hypothesised relationships between these key traits and climate-of-origin (i.e., the climate from where seeds were sourced), investigating the anatomical basis of hydraulic trait variation, and coordination between hydraulic and photosynthetic traits.

In common-environment studies, hydraulic traits often relate to climate-of-origin (from where seeds or seedlings were sourced), with species from drier environments typically exhibiting more negative P_{50} values, indicating greater resistance to embolism (Bourne *et al.*, 2017; Li *et al.*, 2018; Volaire *et al.*, 2018). Similarly, stomatal closure thresholds (g_{s90}), as well as leaf turgor loss point (the water potential at which leaves begin to wilt; Ψ_{TLP}), also tends to decline with aridity (Bourne *et al.*, 2017; Li *et al.*, 2018; Blackman, 2018), such that species from drier sites are able to maintain leaf gas exchange at more negative water potentials during drought. Notably, a global meta-analysis found that stomatal safety margins increase with embolism resistance (Martin-StPaul et al., 2017), indicating that early stomatal closure remains important even in arid-adapted species.

Compared to trait associations with site rainfall, relationships between hydraulic traits and site temperature are less well studied and show inconsistent patterns. While some common garden studies report no relationship between temperature of origin and P_{50} (Li *et al.*, 2018; López *et al.*,

2021), meta-analyses have reported conflicting trends between temperature and leaf P_{50}, ranging from a weak negative relationship (Nardini & Luglio, 2014) to a positive relationship (Huang *et al.*, 2024). Such mixed results may not be surprising given that increased embolism resistance is advantageous both in cold environments, where there is increased risk of freeze-thaw embolism, as well as in hot-dry environments, where there is increased risk of embolism during drought (Davis *et al.*, 1999; Pittermann & Sperry, 2006; Hartill *et al.*, 2023).

Anatomical differences in the water conducting xylem underpin variation in key hydraulic traits, yet their role in modulating variation in hydraulic conductivity and embolism resistance across environmental gradients remains poorly understood. Hydraulic conductivity increases with conduit diameter to the fourth power (Sperry *et al.*, 2006) but wider vessels may be more vulnerable to embolism, as proposed by the hydraulic safety-efficiency trade-off (Tyree *et al.*, 1994), although empirical evidence for the trade-off is mixed (Gleason et al 2016). Wide vessels are advantageous in warm environments, where high evaporative demand necessitates efficient water transport, but are disadvantageous in dry environments, where the risk of drought-induced embolism increases (Olson *et al.*, 2018; Fontes *et al.*, 2022). Vessel wall thickness is also closely linked to embolism resistance (Lens *et al.*, 2016; Li *et al.*, 2016; Volaire *et al.*, 2018), possibly via thicker pit membranes (Li et al., 2016; Thonglim et al., 2021), and may also function as an adaptation to freeze-thaw embolism in cooler climates (Davis *et al.*, 1999).

Much of our current understanding of plant hydraulic traits and their anatomical basis comes from studies of woody species. By contrast, hydraulic traits in herbaceous plants remain comparatively understudied, and their relationships with climate are rarely explored (but see Ocheltree *et al.*, 2016; Volaire *et al.*, 2018; Jardine *et al.*, 2021). Furthermore, while hydraulic traits have been well described across broad taxonomic scales (e.g., Choat *et al.*, 2012; Nardini and Luglio, 2014; Huang *et al.*, 2024), within-species variation, especially in herbaceous species, is not well understood. Grasses dominate over 40% of the Earth's terrestrial surface and are crucial for global agriculture (McSteen & Kellogg, 2022), yet studies of within-species variation in hydraulic and gas exchange traits in grasses from contrasting climates, including the relationship between xylem embolism and stomatal regulation that define different drought response strategies, are lacking.

The traits and processes involved in the survival and recovery of grass species after extreme drought are often complex and multifaceted (Craine *et al.*, 2013; Hoover *et al.*, 2014). Like woody species, perennial grasses from arid environments may exhibit drought tolerance (embolism resistance) or drought avoidance (early loss of turgor and stomatal closure) strategies, but they can also employ alternative mechanisms such as aboveground senescence and/or dormancy to survive

drought (Volaire *et al.*, 2009; Zwicke *et al.*, 2015; Balachowski *et al.*, 2016; Keep *et al.*, 2021). *Themeda triandra Forssk*. is a perennial C_4 tussock grass in the Andropogoneae tribe (which includes major crops like sorghum, maize, and sugarcane) and is the most widespread plant species in Australia (Gallagher, 2016), occurring across all biomes from semi-arid savannas and seasonally wet tropics to sub-alpine and cool temperate regions (Dunning *et al.*, 2017). The exceptional climatic breadth and ecological dominance of this species make it ideal for examining how grasses have evolved diverse strategies to cope with drought and to investigate how variation in hydraulic and other physiological traits are driven by climate adaptation.

In this study *T. triandra* plants were grown from seed sourced from eight populations from sites across the Australian continent strongly contrasting in rainfall and temperature. We measured a range of key hydraulic, photosynthetic and xylem anatomical traits in well-watered plants before characterising their stomatal response to drought. We tested hypothesised relationships between key traits and climate-of-origin rainfall and temperature (see below). We also explored various trait–trait relationships, including those related to the proposed hydraulic safety–efficiency trade-off (Hacke *et al.*, 2006; Gleason *et al.*, 2016; Ocheltree *et al.*, 2016) and the coordination between leaf hydraulics and leaf gas exchange . By investigating hydraulic, anatomical and gas exchange traits across multiple *T. triandra* populations grown under common conditions, this study aims to identify distinct trait-climate associations based on genetic variation without the influence of environmentally-induced plasticity (Jankowski *et al.*, 2019; Huxman *et al.*, 2022; Schwinning *et al.*, 2022). Understanding these within-species patterns in a wild Andropogoneae grass may provide insights for predicting shifts in native grassland composition under climate change and avenues for enhancing drought resilience in related crop species.

Our work tested a number of hypotheses based on fundamental principles of plant hydraulics, and previous empirical trends reported in the literature:

Hypotheses

1. Plants from drier environments exhibit more negative values for P_{50}, Ψ_{TLP}, and g_{s90} and have smaller, thicker-walled vessels and higher vein density.
2. Plants from warmer sites exhibit higher hydraulic conductance (K_{leaf}), linked to wider vessels, enabling more efficient water transport and sustained leaf function under high evaporative demand.
3. Plants with more negative P_{50} have smaller vessels and thicker xylem vessel walls accompanied by lower K_{leaf}, in accordance with an assumed hydraulic safety-efficiency trade-off.

In addition, we expected traits related to rapid resource capture (A_{max}, K_{leaf}, and g_{smax}) to covary positively among themselves but negatively with traits related to stress tolerance (P_{50}, Ψ_{TLP}, and g_{s90}), reflecting a trade-off between distinct adaptive strategies.

Methods

Plant Growth

We grew 10 – 12 replicates of eight populations of *T. triandra*, sourced from diverse climatic regions across Australia (Figure 1, Table S2; summer temperatures ranging from 16.3 – 32.1°C and summer precipitation ranging from 75 – 435 mm), in a climate-controlled glasshouse at the Hawkesbury Institute for the Environment, Western Sydney University, Richmond, NSW. Plants were grown from seeds germinated in seed trays. After emergence they were transplanted into 8-litre pots filled with sandy-loam soil (pH ≈ 5.6) collected from the PACE field facility at Western Sydney University (Churchill *et al.*, 2022). The soil in each pot was supplemented with 10 g of slow-release native-plant fertiliser (Osmocote® Native). Seedlings subsequently received a half-strength application of Yates Thrive® All-Purpose fertiliser (N:P: K 25:5:8), applied weekly for the first four weeks, to prevent nutrient limitation during establishment.

All pots were maintained at 100% field capacity, using an automated irrigation system, for the first two months of growth. The glasshouse was maintained at 30/20°C (day/night) temperatures with ambient CO_2 levels (~420 ppm) and a 14-h light period. Natural light was supplemented throughout the light period with full spectrum LED lighting, adding 700 µmol photons m^{-2} s^{-1}, with maximum midday levels reaching ~1500 µmol photons m^{-2} s^{-1}. Following this initial growth period, all plants underwent a "drought-hardening" pre-treatment, in which watering was withheld for 4 – 5 days, inducing visible leaf wilting. After this period of water deficit, plants were rewatered to 100% field capacity and maintained under these conditions for 4 – 6 days, ensuring full rehydration (predawn leaf water potential ≈ 0). All plants were maintained at 100% field capacity for an additional two weeks before being allocated to two experimental groups: 1) "Steady-State Trait Characterisation" plants were used to measure key hydraulic, physiological and anatomical traits, and 2) "Dynamic Dry-Down Assay" plants were subjected to a progressive dry-down to assess stomatal responses to desiccation.

Steady-State Trait Characterisation

155 *Leaf xylem vulnerability measurements*

156 The optical vulnerability (OV) technique (Brodribb *et al.*, 2016) was used to visualise embolism
157 events and estimate vulnerability thresholds in the leaves of 4 – 5 replicates for each population.
158 Whole individual plants (including root systems) were carefully removed from pots early in the
159 morning and roots were washed to remove any soil. Excised plants were placed in a bucket
160 containing a shallow layer of water and covered with black plastic bags to ensure that they remained
161 well hydrated, so embolism due to dehydration did not occur before OV measurements began.
162 Plants were transported immediately to the laboratory for OV measurements, where a fully
163 expanded leaf from each individual was positioned between two plastic polarising films and placed
164 into a CaviCam clamp. The CaviCam consists of a Raspberry Pi single board computer (Raspberry Pi
165 Foundation, http://www.raspberrypi.org) which controls and stores images produced by an 8-Mp
166 camera magnified by a ×20 lens. Leaf samples were illuminated from below using six light-emitting
167 diodes (LEDs) delivering ~200 µmol quanta m^{-2} s^{-1} to the leaf and providing refracted light from the
168 sample surface to the camera. All components were housed within a 3D-printed clamp (further
169 details of the clamps are provided at https://github.com/OpenSourceOV).

170 Leaf water potential was concurrently measured on the nearest neighbouring leaf using a stem
171 psychrometer (ICT PSY Armidale, NSW, Australia) (Johnson *et al.*, 2018). The psychrometer was
172 automated to take water potential readings every 10 minutes, and the accuracy of the psychrometer
173 was verified for a subset of individuals using a Scholander pressure chamber (PMS Instruments)
174 (Figure S1); leaves of comparable size were used for all individuals for consistency. Both water
175 potential and xylem images were recorded until each plant had dehydrated completely (i.e.
176 embolism events had ceased for >12 hours).

177 Images of xylem embolism were processed using ImageJ using the instructions at
178 https://github.com/OpenSourceOV/image-processing-instructions/blob/master/instructions.md.
179 Differences between neighbouring images in each sequence were used to highlight embolism
180 events. Rapid changes in pixel intensity associated with embolism are distinguishable from other
181 changes in the leaf during dehydration (Johnson *et al.* 2018). Threshold analyses were used to
182 remove noise related to leaf movement, in order to produce a set of images that contain only the
183 pixels associated with embolism events. These data were used to determine the percentage of
184 embolism using the following equation.

$$\%embolism = \frac{A_{emb}}{A_{total}} \times 100,$$

185 Where A_{emb} is the cumulative area of embolised xylem at a given time and A_{total} is the total area of
186 embolised xylem at the end of sample dehydration. Finally, the water potential data were combined
187 with the total cumulative pixel count to create a vulnerability curve for each species.

188

189 *Maximum rates of leaf gas exchange and leaf hydraulic conductance*

190 Steady state measurements of net photosynthesis (A_{sat}; µmol m^{-2} s^{-1}), stomatal conductance (g_s; mol
191 m^{-2} s^{-1}) and transpiration (*E*; mmol m^{-2} s^{-1}) were conducted on 4 – 5 replicates of each population
192 between 09:00 and 12:00 on recently fully expanded leaves using a portable open, infra-red gas
193 exchange system (LI-6800, Li-Cor, Lincoln, NE, USA). Measurements were conducted at a saturating
194 photosynthetic photon-flux density (PPFD) of 1800 mmol m^{-2} s^{-1} and a chamber reference [CO_2] (C_a)
195 of 420 µmol CO_2 mol^{-1} at average daily mid-day temperatures (30°C). Leaf-to-air vapour pressure
196 deficit levels were maintained at roughly 1.5 – 2.0 kPa. Each leaf was allowed ~5 mins to equilibrate
197 before measurements were taken (Ghannoum *et al*. 2010). Well-watered control pots from
198 experiment two were also measured daily until the end of the experiment and A_{sat} and g_s values
199 were averaged across multiple timepoint to calculate g_{smax} and A_{max}.

200 Maximum leaf hydraulic conductance (K_{leaf}) was measured using the "relaxation by rehydration"
201 method (Brodribb & Holbrook, 2003). A pair of adjacent leaves were selected based on comparable
202 size and condition from well-watered individuals (either two leaves from the same tiller or adjacent
203 leaves). The initial leaf water potential (Ψ_0) was measured on the first leaf, using a pressure
204 chamber, and the second leaf was partially submerged in filtered, de-ionized water, and recut at the
205 base and rehydrated for 30 seconds. The apical section of the leaf remained out of the water,
206 ensuring that rehydration occurred only through the cut xylem. After rehydration, the second leaf
207 was re-cut above the water line and placed in a pressure chamber to obtain the final rehydrated leaf
208 water potential (Ψ_f). Leaf hydraulic conductivity (K_{leaf}) was calculated using the following equation.

$$K_{leaf} = \frac{C_{leaf} \ln\left(\left[\frac{\Psi_0}{\Psi_f}\right]\right)}{t}$$

209 where C_{leaf} is the bulk leaf capacitance before turgor loss, normalized by leaf area, t is the duration of
210 rehydration, and Ψ_0 and Ψ_f are the initial and final leaf water potentials, respectively.

211 *Pressure Volume Curves*

212 Pressure-volume curves were conducted on multiple leaves from 4 – 5 individuals from each
213 population to determine turgor loss point (ΨTLP) and C_{leaf}. Leaves were sampled at dusk and placed
214 in opaque plastic bags, with the distal end of each leaf placed under water and left to rehydrate
215 overnight. Rehydrated leaves were photographed, and images were analysed using ImageJ to
216 calculate leaf area. Leaf fresh weight (FW) and Ψ_{leaf} were then periodically measured during slow
217 desiccation, until Ψ_{leaf} reached -3 MPa. Sample leaves were then oven dried at 70°C for a minimum
218 of 48 hr to obtain dry weight (DW). Ψ_{TLP} was calculated by plotting leaf relative water content
219 (RWCleaf, %) against the inverse of Ψ_{leaf}, and Ψ_{TLP} was determined as the point where the line
220 became non-linear. Area-based leaf-specific capacity at full turgor (C_{leaf}) and leaf osmotic potential at
221 full turgor (Ψ_{osm}) were calculated for each individual leaf following standard pressure-volume curve
222 analysis methods (Turner, 1988; Sack et al., 2011) and averaged across replicate leaves of the same
223 plant.

224 *Analyses of xylem characters using light microscopy*

225 Leaf samples from the same individuals used for leaf hydraulic vulnerability measurements were
226 collected and immediately fixed in a 5% formaldehyde, 5% acetic acid, and 70% ethanol solution
227 (FAA) solution for 48 hours to preserve tissue structure. Following fixation, samples were gradually
228 dehydrated through an ethanol series up to 70% for long-term storage before embedding. Fixed
229 samples were embedded in Optimal Cutting Temperature compound (Tissue-Tek® O.C.T. Compound,
230 Sakura Finetek, USA) and sectioned at -25°C and 6 µm thickness using a cryostat (HM525 NX,
231 Epredia). Sections were transferred by gentle pressure contact onto 1.3% Fol's chrom-alum gelatine
232 subbed glass slides (Kiernan, 1999). For staining, sections on slides were first submerged in 1%
233 Safranin O for 10 minutes, to stain lignified tissues. Samples were then dehydrated in 70% ethanol
234 and counterstaining was performed with 0.5% Fast Green (in absolute ethanol). Finally, sections
235 were cleared in xylene and dry specimens were mounted permanently with Eukitt mounting medium
236 (Sigma-Aldrich).

237 Images from each population were captured using an Axiocam 503 colour module (Zeiss) attached to
238 an Axioscope 5 (Zeiss) microscope under a phase contrast setup. Leaf anatomical traits were
239 quantified via image analysis using Fiji, ImageJ2 (ImageJ v. 1.54f). Measured traits included vein
240 density and diameter for both major and minor veins, and metaxylem vessel wall thickness for major
241 veins. For each replicate, two measurements were taken and the mean reported. Vein diameter was
242 quantified as the tangential diameter of the two largest vessels, measured at the widest point of the
243 lumen (excluding cell walls), and expressed as arithmetic means. Vessel wall thickness was measured
244 on metaxylem vessels in major veins. Vein density was determined by counting individual major and

minor veins per leaf section and normalizing by leaf section length (veins cm^{-1}), determined using a white reference line along the blade margin. Further methodological details, measurement protocols and representative images, are provided in Table S4.

Dynamic Dry-Down Assay

One replicate pot from each population was maintained at 100% field capacity to serve as the well-watered control while four other replicates of each population were subjected to a prolonged, severe dry-down by completely withholding irrigation. Soil moisture was measured daily using a handheld soil water reflectometer (HydroSense II CS659, Campbell Scientific). Predawn (Ψ_{PD}) and midday (Ψ_{MD}) leaf water potentials were also measured daily, using a Scholander pressure bomb (PMS Instruments, Albany, OR, USA) fitted with a grass compression gland and base, on two to three leaves per individual to track plant water status. Concurrently, daily measurements of light-saturated photosynthesis (A_{sat}; µmol m^{-2} s^{-1}), stomatal conductance (g_s; mol m^{-2} s^{-1}) and transpiration (*E*; mmol m^{-2} s^{-1}) were taken on the same leaves. These data were used to derive the leaf water potential at 90% stomatal closure (g_{s90}). Steady state measurements of A_{sat}, g_s and *E* were conducted between 09:00 and 12:00 on recently fully expanded leaves using the LI-6800 (described above). Measurements were conducted at a saturating PPFD of 1800 mmol m^{-2} s^{-1} with a chamber reference [CO_2] (C_a) of 420 µmol CO_2 mol^{-1} and at average daily midday temperatures (30°C). Leaf-to-air vapour pressure deficit levels were maintained at roughly 1.5–2.0 kPa. Each leaf was allowed ~5 mins to equilibrate before measurements were taken. Measurements were conducted daily on the dehydrating pots (on 2 – 3 leaves from each individual plant per day) until stomatal closure occurred (i.e. g_s was reduced by > 90%). All parameters were also measured on well-watered control pots until the end of the experiment.

Climate data

T. triandra occurs across a variety of climate zones in Australia. To identify the most appropriate climate-of-origin descriptors for this comparative study, ten climatic variables capturing temperature and precipitation means, seasonality, and extremes for each of the eight source locations were extracted from CHELSA gridded datasets (Karger *et al.*, 2017), which report long-term (1981 – 2010) interpolated climate averages at a spatial resolution of ~ 1km at the equator. Principal components analysis was used to identify the major tendencies across these ten variables, with varimax rotation applied to improve interpretability (aligning climate vectors more clearly with individual factors rather than composite mixtures). The first rotated axis reflected a temperature–seasonality gradient (driven by temperature range and mean summer temperature). The second axis captured a

277 precipitation gradient (driven by summer and annual precipitation). From these analyses we
278 selected *summer temperature* and *summer precipitation* as the key climate variables to be used in
279 analysis of trait – climate relations. These two variables had the strongest loadings (Table S3) on
280 their respective axes and have clear biological relevance given this perennial species exhibits peak
281 growth during the warmer summer months, especially in colder regions where its growth is
282 restricted to this period (Snyman *et al.*, 2013; Churchill *et al.*, 2022). Summer temperature and
283 summer precipitation vary almost independently across our eight populations (R^2 = 0.03, P = 0.698),
284 allowing their use in subsequent models. Note, we used statistical approaches (described below)
285 that simultaneously considered the effects of two climate variables, allowing us to quantify trait
286 relationships with summer temperature *with variation in summer rainfall held constant*, and vice
287 versa.

288 *Statistical Analysis*

289 Leaf hydraulic vulnerability curves were fitted using the "fitplc" function from the "fitplc" package
290 (Duursma & Choat, 2017), using Weibull models where they converged and sigmoidal models when
291 curves exhibited abrupt, steep declines in conductance that caused non-linear optimisation to break
292 down. Individual vulnerability curves were generated for each replicate plant and the leaf water
293 potentials causing 12% (P_{12}) and 50% (P_{50}) xylem embolism were quantified. Stomatal conductance
294 values were plotted against leaf water potential and fitted with a weighted polynomial regression,
295 using the "*fitcond*" function within the "*fitplc*" package, to extract leaf water potential at stomatal
296 closure (g_{s90}). Stomatal safety margins (MPa) were calculated as the difference between the Ψ_{MD} at
297 which stomata were 90% closed (g_{s90}) and P_{50} (SSM).

298 To assess the relationship between plant functional traits and the two climate variables, we used
299 linear mixed-effects models fitted with the "lme4" package in R. The model structure included a
300 response variable (trait of interest) as a function of climate predictors. To incorporate the repeated
301 sampling structure of the data, the site of origin for each population was specified as a random
302 effect:

$$model = trait \sim Summer\ Precip + Summer\ Temp + (1|Accession)$$

303 A corresponding fixed-effects linear model was also fit without the random effect for visualization of
304 partial residuals. We also tested for an interaction between summer precipitation and summer
305 temperature for each trait but found no significant interactions, so we retained an additive model
306 structure. The effect of each climate predictor on the response trait was visualized using the "visreg"
307 package, extracting model residuals to generate partial residual plots. This approach allows for the

visualization of the independent effects of precipitation and temperature on the trait of interest while accounting for the influence of other variables in the model. P-values for fixed effects were quantified using the "lmerTest" package.

To assess the robustness of our findings, we also conducted bivariate analyses of each climate variable independently. This approach allowed us to examine whether incorporating both precipitation and temperature in the mixed model influenced our results by accounting for covariation between these climate factors. Additionally, bivariate analysis strengthens our results by providing a complementary perspective on trait-climate relationships, helping us determine which correlations remain consistent across different analytical approaches. Moreover, we included an annual moisture index (calculated as precipitation/potential evapotranspiration) in our bivariate analysis, this being a widely used, an integrated measure of site water availability.

Results

Leaf hydraulic conductance (K_{leaf}) varied markedly among *T. triandra* populations, ranging from an average of 2.53 mmol m^{-2} s^{-1} MPa^{-1} at Sydney to 11.10 mmol m^{-2} s^{-1} MPa^{-1} at Virginia (Table. S5). Xylem embolism resistance (P_{50}) also varied clearly among populations, ranging from -2.41 MPa in plants from Hobart (southern Australia) to -5.13 MPa (Fig. S2) in plants from Pannawonica (north-western Australia). Traits governing plant water status showed less variation across populations, with mean turgor loss point (Ψ_{TLP}) ranging from -1.17 to -1.86 MPa and stomatal closure (g_{s90}) ranging from -3.93 to -5.44 MPa. Stomatal safety margins (SSM = P_{50} - g_{s90}) ranged from +0.75 MPa; Forbes) to -1.54 MPa; Mt Fox National Park)., with positive and negative values indicating that stomatal closure occurs before and after the onset of 50% embolism, respectively.

Trait relationships with climate-of-origin

We predicted (Hypothesis 1) that populations from drier sites would be more resistant to water stress, displaying more negative P_{50} and Ψ_{TLP} values than those from wetter sites. Instead, we found that P_{50} and precipitation were unrelated (Fig. 2A), while drier-site populations exhibited less negative Ψ_{TLP} (Fig. 2C). These findings were supported by both the LMM and bivariate analyses (Table S1). Drier-site populations exhibited a suite of drought-avoidance traits, including stomatal closure at less negative water potentials (g_{s90}) and wider stomatal safety margins (SSM) (Fig. 2G). K_{leaf}

338 was significantly higher in drier-site populations (Fig. 2I). Neither of the SSM or K_{leaf} trends were
339 observed in bivariate analyses (Table S1).

340 Using LMM analysis, populations originating from warmer climates exhibited greater drought
341 tolerance, as indexed by more negative P_{50} (Fig. 2B). However, Ψ_{TLP} (Fig. 2D) and g_{s90} (Fig. 2F) were
342 unrelated to climate-of-origin temperature. These tendencies were also observed in bivariate trait–
343 temperature analyses (Table S1). The positive relationship between temperature and P_{50} indicated a
344 tendency for plants from warmer climates to exhibit higher SSMs than plants from cooler climates
345 (Fig. 2H), although this was observed in the LMM analysis only. In support of Hypothesis 2, warm-
346 origin plants had significantly higher K_{leaf} than cool-climate plants (Fig. 2J), if in the LMM analysis only
347 (Table S1).

348 Moisture Index (the annual balance between precipitation and potential evapotranspiration) at the
349 climate of origin had little relationship to hydraulic traits except that plants from more arid
350 environments exhibited marginally higher hydraulic conductance than those from mesic sites (P =
351 0.067; Table S1).

352 Counter to expectations (H3), neither vessel diameter (in major or minor veins) nor vessel wall
353 thickness varied with climate-of-origin rainfall, whether considered simultaneously with
354 temperature variation (LMMs: Figs 3A, E, I) or in bivariate analyses (Table S1). Vessel density
355 (number per cross-sectional area) was also unrelated to precipitation (Fig. 3C, G; Table S1).
356 Relationships with site temperature differed between vein types: major vein traits were unrelated to
357 temperature (Fig. 3B, D; Table S1), whereas minor vein traits showed distinct temperature-driven
358 trends. Plants from warmer sites had wider minor vein vessels (Fig. 3F) and reduced minor vein
359 density compared to cooler sites (Fig. 3H). The same trends were also evident in bivariate trait–
360 climate analyses (Table S1). Moisture Index was not correlated with vessel diameter (both minor and
361 major veins) but plants from more arid sites had lower minor vein density than those from more
362 mesic sites (P = 0.049 Table S1).

363

364 In LMMs, g_{smax} was significantly higher in plants from wetter environments (Fig. 4C) and marginally
365 higher in plants from colder sites (Fig 4D), however, A_{max} was not significantly related to climate-of-
366 origin rainfall or temperature (Fig. 4A, B). These relationships were consistent in bivariate trait-
367 climate analyses (Table S1).

368

369 **Coordination among hydraulic, anatomical, and photosynthetic traits**

The expected trade-off (Hypothesis 3) between hydraulic safety (P_{50}) and hydraulic efficiency (K_{leaf}) was not supported (Fig. 5A). Variation in P_{50} was also unrelated to A_{max} and g_{smax} (Fig. 5C, D). Notably, populations with lower Ψ_{TLP} typically had lower g_{smax} ($R^2 = 0.55$, $P < 0.036$; Fig. 5H) and marginally lower A_{max} ($R^2 = 0.45$, $P = 0.067$; Fig. 5I). Contrary to expectations (Hypothesis 3), plants that were more resistant to embolism (more negative P_{50}) also had wider major vein xylem vessels ($R^2 = 0.61$, $P = 0.023$; Fig. 6A) and wider minor vein xylem vessels ($R^2 = 0.52$, $P = 0.043$; Fig. 6C). Plants with more negative P_{50} also exhibited lower minor vein density ($R^2 = 0.48$, $P = 0.056$; Fig. 6D), but there was no relationship with major vein density (Fig. 6B). Vessel wall thickness was unrelated to P_{50} (Fig. 6E). Variation in hydraulic conductivity (K_{leaf}) was largely unrelated to xylem anatomy, except that plants with lower minor vein density had higher K_{leaf} ($R^2 = 0.79$, $P = 0.003$; Fig. 6I). We found no evidence of coordination between xylem embolism resistance (P_{50}) and stomatal closure (g_{s90}; Fig. 7A, C, E) or turgor loss point (Ψ_{TLP}; Fig. 7B, D). However, Ψ_{TLP} exhibited a significant positive relationship with g_{s90} (Fig. 7E), consistent with the role of turgor loss in constraining stomatal closure during dehydration. K_{leaf} was strongly negatively related to both A_{max} (Fig. 8A) and g_{smax} (Fig. 8B), contrasting with a simple supply–demand coupling between hydraulic conductance and gas exchange capacity in this species.

Discussion

Our study of key hydraulic, anatomical, and photosynthetic traits measured in eight populations of *T. triandra* selected from diverse climatic regions across Australia revealed contrasting trait syndromes associated with climate-of-origin precipitation and temperature. Our results challenge commonly assumed trait trade-offs, suggesting a more nuanced coordination of hydraulic function and gas exchange traits across populations of this widespread grass species. These findings provide insight into how diverse hydraulic strategies emerge within a single species and highlight key traits that may enhance drought resistance and resilience under future climates.

High hydraulic conductance and embolism resistance in warmer climates

Consistent with our second hypothesis, plants from warm sites exhibited generally higher hydraulic conductance, aligning with previous findings in woody angiosperms (Nardini & Luglio, 2014; Larter *et al.*, 2017; Peters *et al.*, 2021). Plants growing in hot, high-VPD environments may require greater hydraulic capacity to match elevated evaporative demand under such conditions (Brodribb & Jordan, 2008; Osborne & Sack, 2012; Scoffoni *et al.*, 2016). Beyond maintaining plant water balance, higher K_{leaf} also facilitates greater leaf transpirational cooling in hot environments (Blonder *et al.*, 2023). Notably, plants from warmer sites also exhibited more negative P_{50}, suggesting increased embolism resistance is adaptive where high evaporative demand and increased transpiration generate strongly negative xylem water potentials. This pattern of increasing embolism resistance with increasing

403 temperature has been documented in other herbaceous (Ocheltree *et al.*, 2016; Huang *et al.*, 2024,
404 p. 202) and woody species (Trueba *et al.*, 2017; Guan *et al.*, 2023), as well as in different
405 provenances of the tree species *Corymbia calophylla* (Blackman *et al.*, 2017). However, temperature-
406 P_{50} relationships in woody species vary considerably across studies, with some finding no
407 relationship (Larter *et al.*, 2017; Li *et al.*, 2018; López *et al.*, 2021; Peters *et al.*, 2021) or even
408 negative correlations on a global scale (Nardini & Luglio, 2014). This variation may partly reflect
409 confounding effects of temperature and precipitation, making it difficult to isolate the independent
410 effects of each climate variable. In our study, low collinearity between these factors allowed us to
411 separate their independent effects. Additionally, variation in temperature-P_{50} relationships may
412 reflect different selective pressures operating at temperature extremes, whereby high embolism
413 resistance protects against water stress-induced cavitation in hot environments and against freeze-
414 thaw induced embolism in very cold environments (Davis *et al.*, 1999; Pittermann & Sperry, 2006;
415 Hartill *et al.*, 2023). Since the *T. triandra* populations in our study originated from regions that rarely
416 see severe freezing events during the growing season, the observed increase in embolism resistance
417 with increasing temperature likely reflects adaptations to hydraulic stress due to high VPD in warm
418 climates rather than to freeze-thaw embolism tolerance in cooler climates.

419 Plants from warmer sites exhibited larger minor vein vessels (whereas precipitation was
420 unrelated to anatomical traits). These patterns accord with our second hypothesis and mirror
421 observations in woody species where temperature—but not precipitation—predicted vessel
422 diameter (Morris *et al.*, 2018; Olson *et al.*, 2018), suggesting stronger temperature-driven selection
423 on leaf xylem architecture. Larger vessels may be advantageous in warmer environments with high
424 transpirational demand, as small increases in conduit size can yield large increases in vascular
425 hydraulic conductance according to the Hagen-Poiseuille relationship (Sperry *et al.*, 2006). However,
426 we did not observe a corresponding increase in total K_{leaf} with vessel diameter, likely because total
427 K_{leaf} integrates conductance across both xylem and outside-xylem pathways, with the latter typically
428 representing the dominant hydraulic bottleneck (Scoffoni *et al.*, 2023).

429 ***Conservative water use and efficient water transport in dry environments***

430 Our finding that leaf P_{50} was not related to precipitation did not accord with our first hypothesis or
431 numerous cross-species studies that have reported increased embolism resistance in drier
432 environments (Nardini & Luglio, 2014; Blackman *et al.*, 2014; Bourne *et al.*, 2017; Li *et al.*, 2018;
433 Volaire *et al.*, 2018; Yao *et al.*, 2021). However, intraspecific studies frequently reveal weak or absent
434 correlations between P_{50} and precipitation (Martínez-Vilalta *et al.*, 2009; Bayramzadeh *et al.*, 2011;
435 Lamy *et al.*, 2014; Blackman *et al.*, 2017; López *et al.*, 2021), suggesting that populations from drier

436 climates make adjustments in other traits (e.g., sapwood-to-leaf area ratio (Huber value), stem
437 hydraulic conductivity) that help maintain water potentials within safe limits. Nevertheless, the lack
438 of a P_{50}-precipitation relationship in *T. triandra* parallels patterns observed in nine C_4 grass species
439 (Ocheltree *et al.*, 2016) and may reflect differences in drought response strategies between woody
440 plants and grasses. Woody species (especially evergreens) generally maintain the same conductive
441 tissues through successive periods of water deficit, exposing them to repeated embolism risk. In
442 contrast, grasses such as *T. triandra* can senesce above-ground organs during drought and resprout
443 via basal meristems once drought is alleviated (Volaire *et al.*, 2009; VanderWeide *et al.*, 2014),
444 reducing the need to maintain embolism-resistant tissues.

445 Although we did not observe a significant correlation between P_{50} and climate of origin
446 precipitation, populations from drier sites closed their stomata at less negative water potentials
447 during drought than populations from wetter sites. This earlier stomatal closure in effect increased
448 the stomatal safety margin for drier-site populations (Fig. 2E), indicating a more conservative water
449 use strategy, favouring drought avoidance over tolerance. The observation of less negative g_{s90}
450 values in dry-site *T. triandra* populations aligns with findings among closely-related *Caragana* shrub
451 species (Yao *et al.*, 2021) but contrasts with patterns documented in Australian trees, in which
452 stomatal closure generally occurs at more negative water potentials in drier climates (Bourne *et al.*,
453 2017; Li *et al.*, 2018). Our observation of less negative Ψ_{TLP} in dry-site populations is opposite in sign
454 to the relationship reported from several comparative studies across predominantly woody taxa
455 (Mitchell & O'Grady, 2015; Bourne *et al.*, 2017) yet this discrepancy aligns with evidence that
456 relationships between turgor loss and climate can differ between species (López *et al.*, 2021) and are
457 weak within grasses (Ocheltree *et al.*, 2016). .

458 *T. triandra* plants from drier climates exhibited higher K_{leaf} than those from wetter climates.
459 While this pattern runs counter to general trends in woody species (Nardini & Luglio, 2014) it is
460 consistent with findings in closely related *Caragana* species (Yao *et al.*, 2021) and within *Pinus*
461 *canariensis* (López *et al.*, 2016). Higher K_{leaf} in dry-site populations may enhance the capacity of
462 shallow-rooted grasses to capitalise on brief rainfall pulses in otherwise water-limited environments.
463 Plants from dry sites also exhibited significantly lower rates of $g_{s\,max}$, which may be an adaptation to
464 mitigate water loss from high VPD and low water availability. Taken together, these patterns suggest
465 that *T. triandra* populations from drier climates employ a drought-avoidance strategy characterised
466 by earlier turgor loss and stomatal closure, higher K_{leaf}, and reduced operating stomatal
467 conductance—traits that together minimise exposure to critically low water potentials while
468 maximising the capacity to exploit transient increases in soil moisture.

469

470 ***Coordination among hydraulic traits***

471 Although empirical evidence is mixed, in the sapwood of woody species it is often assumed there is a
472 trade-off between xylem hydraulic safety and efficiency, whereby more conductive wider vessels are
473 inherently more vulnerable to cavitation (Hacke *et al.*, 2006; Gleason *et al.*, 2016). The same
474 principle for a trade-off exists in leaves and has been observed in some groups of species (Nardini &
475 Luglio, 2014; Blackman *et al.*, 2024) but not others (Chen *et al.*, 2009; Hao *et al.*, 2013). Here, P_{50} and
476 K_{leaf} were unrelated across populations (Fig. 5A); moreover, plants from warmer sites exhibited both
477 high embolism resistance and high K_{leaf}.

478 Variation in K_{leaf} was also unrelated to the diameter of major and minor vein vessels and was
479 negatively correlated with minor vein density. This was unexpected considering that high K_{leaf} is
480 typically associated with wide vessels (Sperry *et al.*, 2006; Zanne *et al.*, 2010) and high vein density
481 (Brodribb *et al.*, 2007). Our observations suggest that leaf hydraulic function in *T. triandra* may be
482 primarily determined by outside-xylem factors rather than xylem vessel anatomy. In leaves, outside-
483 xylem pathways have been shown to contribute substantially to hydraulic conductance and
484 influence leaf hydraulic decline during drought (Scoffoni *et al.*, 2023). Because reductions in outside-
485 xylem conductance (K_{ox}) are generally recoverable (Scoffoni et al., 2014; Zhang et al., 2016), while
486 xylem embolism is not (Skelton *et al.*, 2017; Johnson *et al.*, 2018), loss of K_{ox} may act as a protective
487 buffer, decoupling leaf hydraulic safety from efficiency. Consistent with this mechanism, K_{leaf} has
488 been reported to decline well before the onset of xylem embolism in other herbaceous species
489 (Corso *et al.*, 2020; Yao *et al.*, 2021), including *T. triandra* (Jacob *et al.*, 2022).

490 Turgor loss point (Ψ_{TLP}) was strongly coordinated with g_{s90} (Fig. 7E), reinforcing loss of cell
491 turgor as a key driver of stomatal closure (Bartlett *et al.*, 2012, 2014). The combination of low g_{smax}
492 and early loss of turgor in *T. triandra* plants from dry sites suggests a coordinated strategy to
493 conserve water under water limiting conditions. P_{50} and g_{s90} were unrelated, contrasting with the
494 idea that stomatal downregulation under drought is caused by embolism-induced reductions in K_{leaf}
495 (Nardini & Salleo, 2000; Brodribb & Holbrook, 2003; Bartlett *et al.*, 2016). Instead, our results are
496 consistent with recent studies on herbaceous species which also observed no coordination between
497 xylem embolism and stomatal closure (Corso *et al.*, 2020; Jacob *et al.*, 2022).

498

499 ***Hydraulic constraints on leaf gas exchange relaxed by C_4 metabolism.***

K_{leaf} was negatively correlated with maximum stomatal conductance (g_{smax}) and photosynthetic capacity (A_{max}). While this contrasts with the positive coordination between hydraulic and photosynthetic traits sometimes reported in C_3 species (Franks, 2006; Brodribb & Holbrook, 2006; Mitchell *et al.*, 2014; Xiong *et al.*, 2018), it is consistent with work on other C_4 grasses, in which K_{leaf} and leaf gas exchange traits were found to be unrelated (Ocheltree *et al.*, 2016; Zhou *et al.*, 2020; Pathare *et al.*, 2020; Baird *et al.*, 2025). It seems that C_4 grasses may not require high K_{leaf} to sustain photosynthetic rates (unlike in C_3 species), as their carbon-concentrating mechanism allows high photosynthesis despite lower g_s and less negative operating Ψ_{leaf} (Taylor *et al.*, 2011; Zhou *et al.*, 2020; Baird *et al.*, 2025). Additionally, traits unique to C_4 metabolism — such as variation in bundle sheath leakiness — may alter the balance between carbon gain and water movement. Species with low bundle sheath leakiness have the ability to maintain high photosynthetic rates even when the hydraulic conductance is low (Fravolini, 2002). The decoupling may also reflect the pulse-driven environments many C_4 grasses occupy, where the need for maintaining hydraulic safety during dry periods and rapidly maximising carbon gain after rainfall further weaken correlations between K_{leaf} and A_{max}.

Conclusion

Hydraulic strategies of the widespread perennial grass *T. triandra* highlight the complex interplay between hydraulic traits, stomatal regulation and xylem anatomy in shaping climate adaptation. Our findings indicate that populations from drier climates exhibit traits associated with conservative water-use and drought avoidance, displaying lower stomatal conductance, less negative g_{s90}, less negative Ψ_{TLP} and larger stomatal safety margins than wetter-site populations. By contrast, plants from warmer climates exhibited a combination of high hydraulic conductance and high embolism resistance, enabling rapid water transport to match periods of high evaporative demand, while reducing the risk of hydraulic failure. Our results reveal substantial within-species variation in hydraulic traits and provide a more nuanced understanding of the mechanisms enabling success in dry and hot environments that may help inform vegetation models aimed at predicting plant responses to intensifying drought and warming in grassland ecosystems.

Acknowledgements

We thank Dr Alan Humphries from the Australian Pastures Genebank for advice on germinating *T. triandra* and for providing seed sources that helped make this project possible. VKJ, IJW, CJB, EF, ACL TB and ES acknowledge support from the Australian Research Council (CE200100015).

Competing interests

No competing interests are declared.

Author contributions

VJ and IJW led project design, experimental work, and manuscript preparation, with strong support from CJB and BC. ACL, TB, and ES assisted with data collection. All authors discussed results, contributed ideas and text to multiple versions of the manuscript, and approved the final version.

Figures and Tables

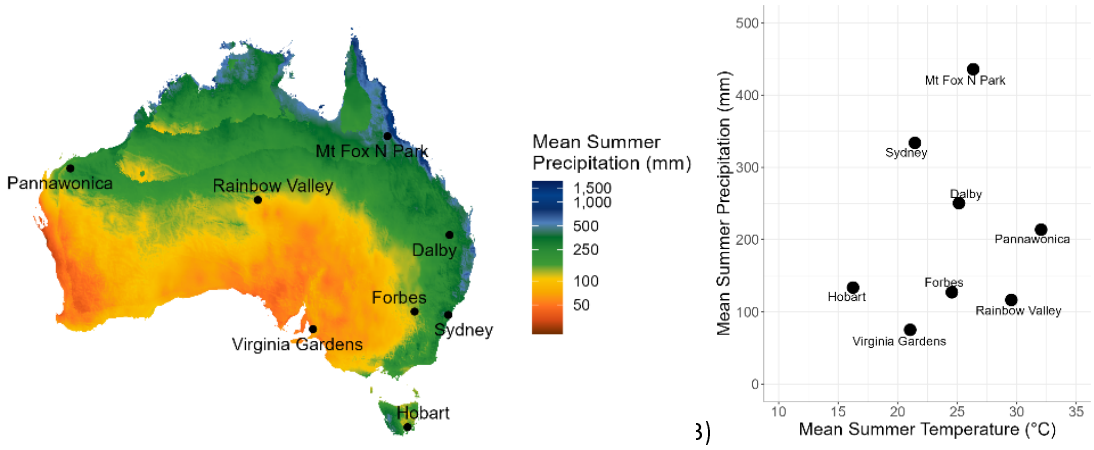

(A) (B)

FIGURE 1. Climate-of-origin of populations used in this study. (A) Mean summer precipitation; mm) across Australia; populations represented by black dots (•). (B) Scatter plot illustrating the two key climatic predictors, with summer temperature (°C) on the x-axis and mean summer precipitation on the y-axis.

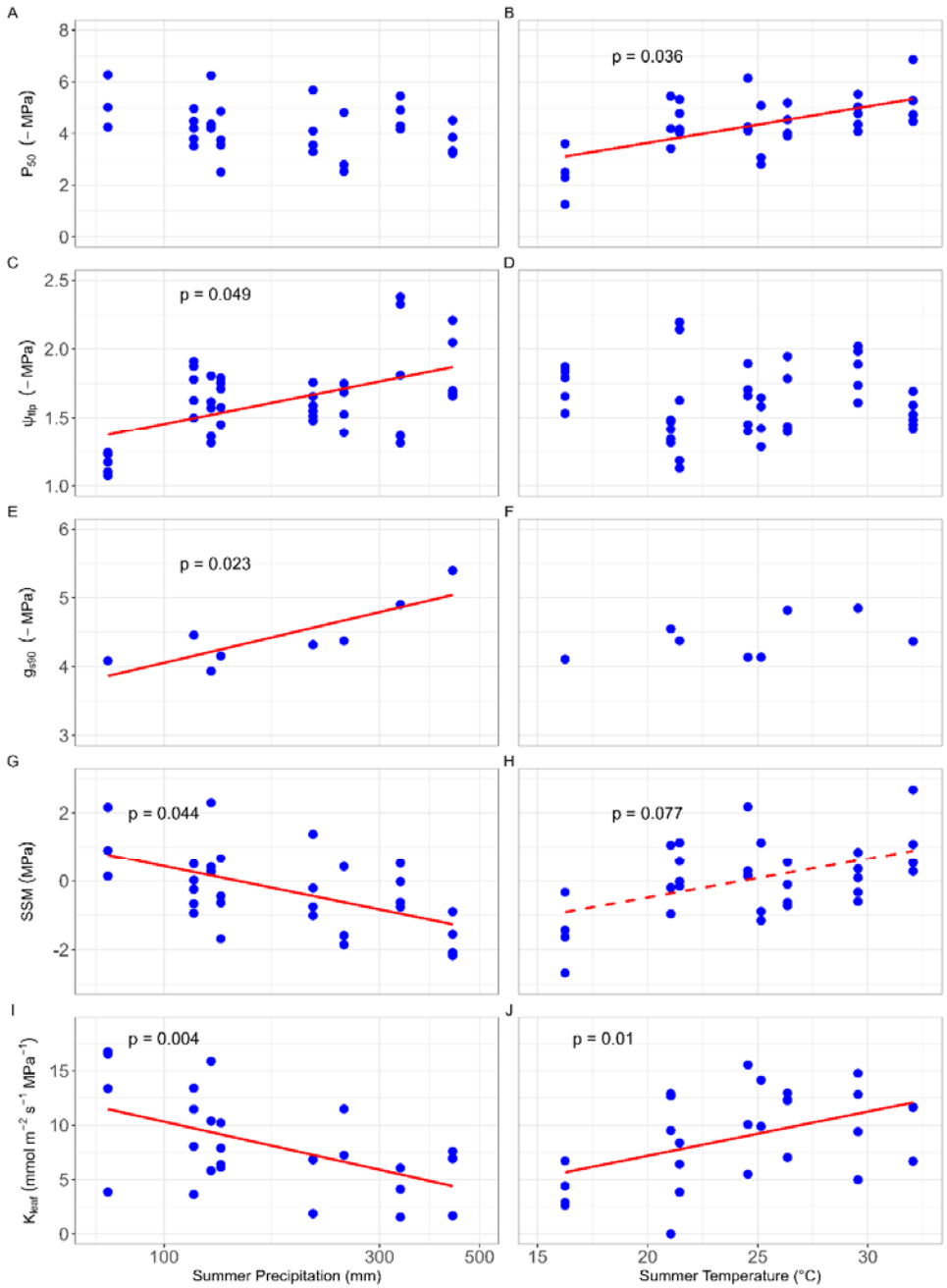

Figure 2. Partial residual plots showing the independent relationships between climate-of-origin and hydraulic traits across populations of *T. triandra*. Relationships between mean summer precipitation (A, C, E, G, I) and mean summer temperature (B, D, F, H, J) with (A, B) water potential at 50% xylem embolism (P_{50}), (C, D) water potential at leaf turgor loss (Ψ_{TLP}), (E, F) water potential at 90% stomatal closure (g_{s90}), (G, H) stomatal safety margin (SSM, Δg_{s90} & P_{50}), and (I, J) leaf hydraulic conductance (K_{leaf}). Fitted lines are derived from linear mixed-effects models using mean data from individual plants, with population as a random effect. Partial residuals were obtained from a corresponding multiple regression model, without the random effect, to visualize the independent effects of each climate variable. Solid red lines indicate significant linear regression fits ($p < 0.05$), while dashed red lines denote marginally significant relationships ($p < 0.1$). Mean summer precipitation was log-transformed to standardize coefficients and back-transformed for visualization.

547

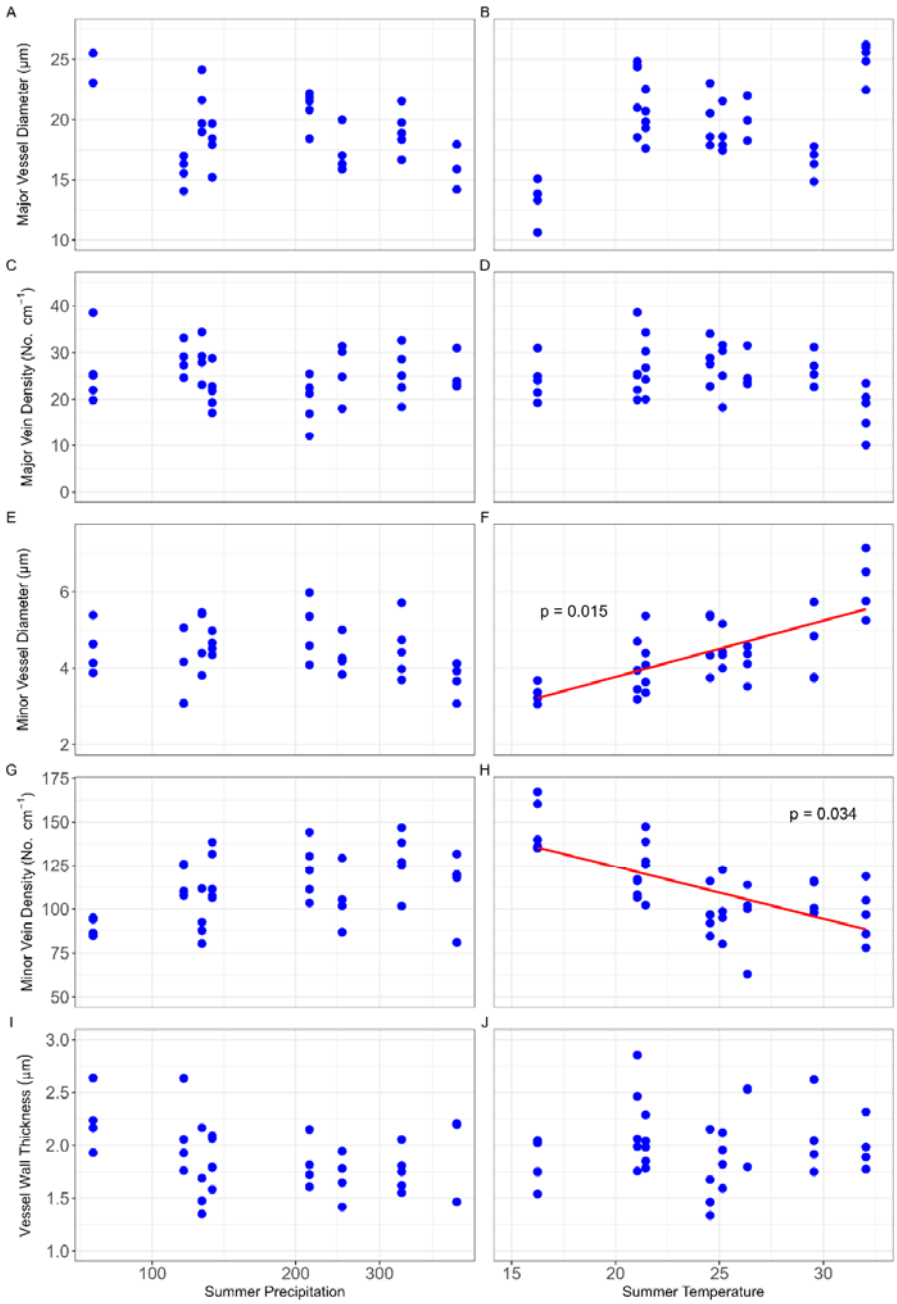

Figure 3: Partial residual plots showing the independent relationships between climate-of-origin and xylem anatomical traits across populations of *T. triandra*. Relationships between mean summer precipitation (A, C, E, G) and mean summer temperature (B, D, F, H) with (A, B) major vessel diameter, (C, D) major vein density, (E, F) minor vessel diameter and (G, H) minor vein density. Fitted lines are derived from linear mixed-effects models using mean data from individual plants, with population as a random effect. Partial residuals were obtained from a corresponding multiple regression model, without the random effect, to visualize the independent effects of each climate variable. Solid red lines indicate significant linear regression fits ($p < 0.05$). Mean summer precipitation was log-transformed to standardize coefficients and back-transformed for visualization.

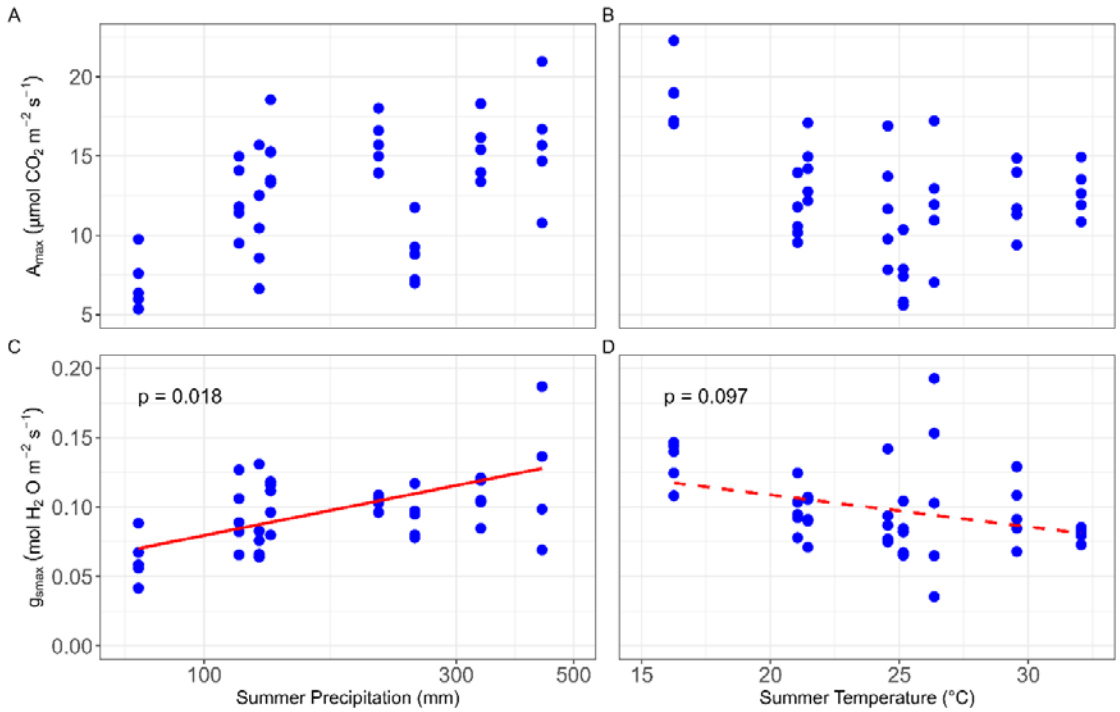

Figure 4. Partial residual plots showing the independent relationships between climate-of-origin and leaf gas exchange traits across populations of *T. triandra*. Relationships between mean summer precipitation (A, C) and mean summer temperature (B, D) with (A, B) maximum rates of light saturated photosynthesis (A_{max}), (C, D) and maximum rates of stomatal conductance (g_{smax}). Fitted lines are derived from linear mixed-effects models using mean data from individual plants, with population as a random effect. Partial residuals were obtained from a corresponding multiple regression model, without the random effect, to visualize the independent effects of each climate variable. Solid red lines indicate significant linear regression fits ($p < 0.05$), while dashed red lines denote marginally significant relationships ($p < 0.1$). Mean summer precipitation was log-transformed to standardize coefficients and back-transformed for visualization.

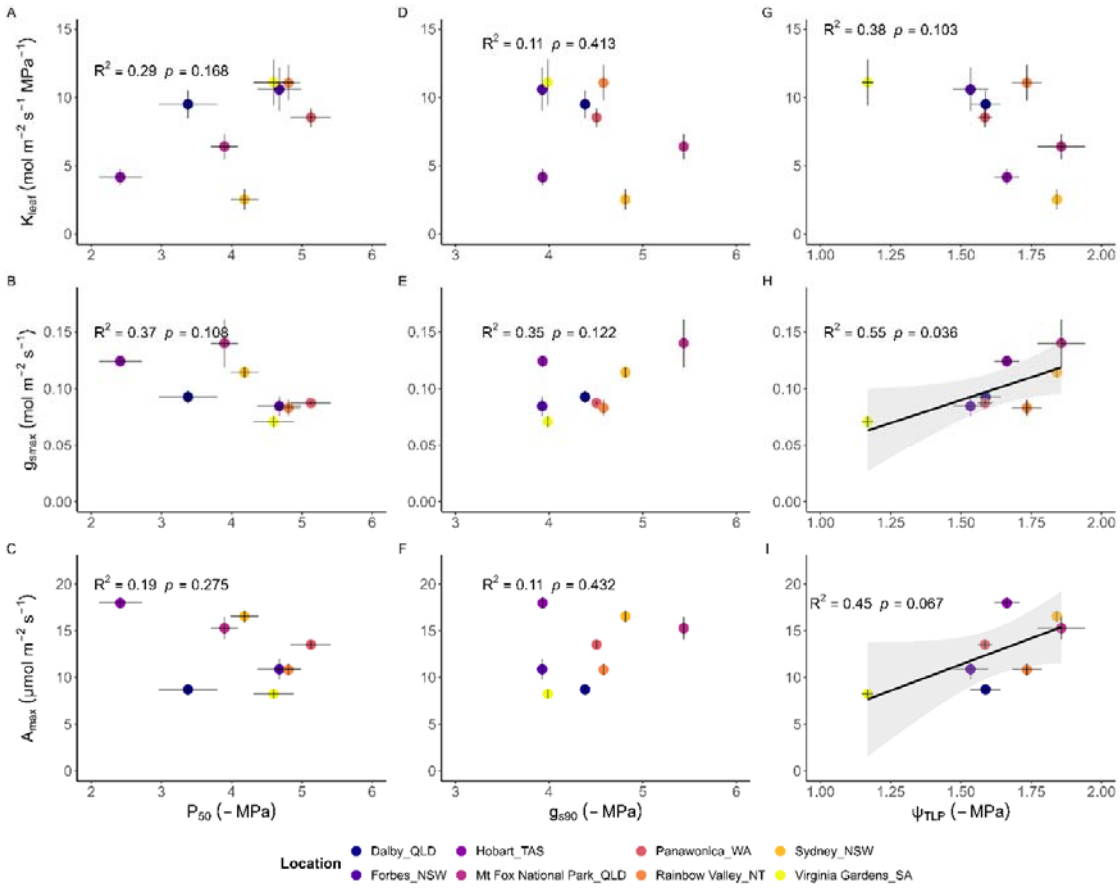

Figure 5: Linear regressions examining relationships between *safety* and *efficiency* traits across populations of *T. triandra*. Correlation between xylem embolism resistance (P_{50}) and (A) hydraulic conductivity (K_{leaf}), (B) maximum stomatal conductance (g_{smax}) and (C) maximum photosynthetic rate (A_{max}). Relationships between xylem water potential at 90% stomatal closure (g_{s90}) and (D) K_{leaf}, (E) g_{smax} and (F) A_{max}. Relationship between leaf water potential at turgor loss (Ψ_{TLP}) and (G) K_{leaf}, (H) g_{smax} and (I) A_{max}. Solid lines and shaded 95% confidence bands are displayed only for statistically significant relationships ($P < 0.1$). Adjusted R^2 values and P-values (derived from Pearson correlations, equivalent to simple OLS tests) are likewise displayed only when $p < 0.1$. Error bars denote ± standard error of the mean; colours denote different populations.

562

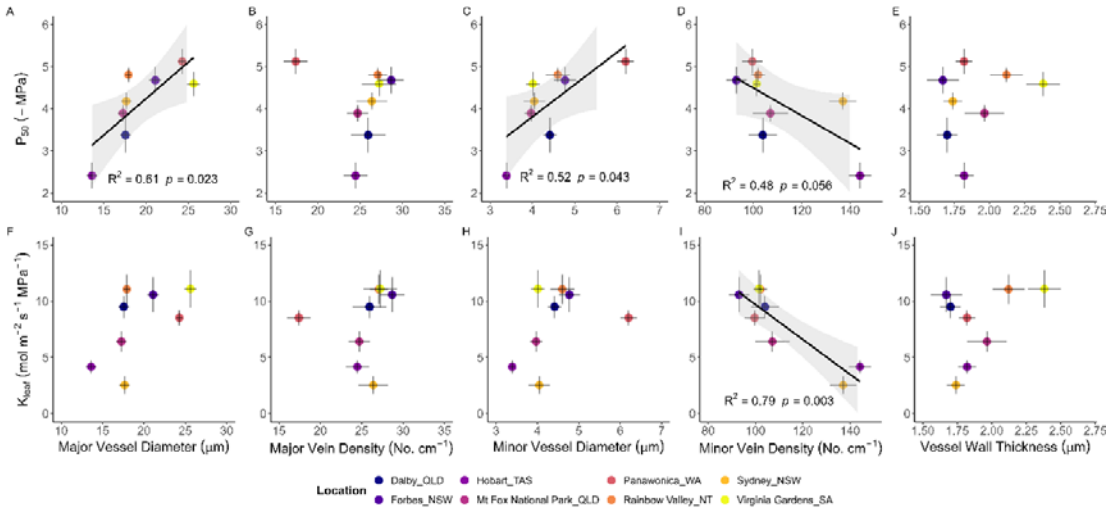

Figure 6: Linear regressions examining relationships between hydraulic traits and xylem anatomy across populations of *T. triandra*. (A–E) Correlations between xylem embolism resistance (P_{50}), (F–J) leaf hydraulic conductance (K_{leaf}) and major vessel diameter (A, F), major vessel density, (B, G) minor vessel diameter (C, H), minor vein density (D, I), and major vessel wall thickness (E, J). Solid lines and shaded 95% confidence bands are displayed only for statistically significant relationships ($P < 0.1$). Adjusted R^2 values and P-values (derived from Pearson correlations, equivalent to simple OLS tests) are likewise displayed only when $p < 0.1$. Error bars denote ± standard error of the mean; colours denote different populations.

563

564

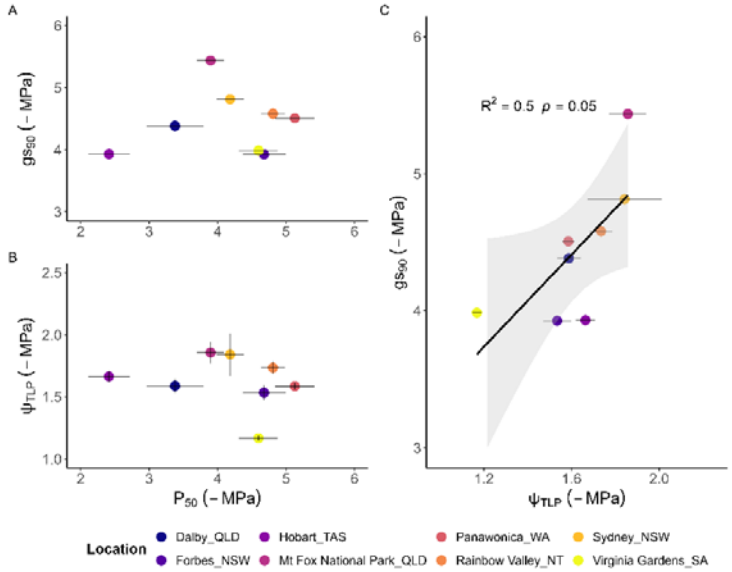

Figure 7. Linear regressions examining relationships between hydraulic vulnerability and water potential at turgor loss and stomatal closure across *T. triandra* populations. Correlations between water potential at 50% xylem embolism (P_{50}) and (A) water potential at 90% stomatal closure (g_{s90}) and (B) leaf water potential at turgor loss (Ψ_{TLP}). Correlation between Ψ_{TLP} and (E) g_{s90} . Solid lines and shaded 95% confidence bands are displayed only for statistically significant relationships ($P < 0.1$). Adjusted R^2 values and P-values (derived from Pearson correlations, equivalent to simple OLS

tests) are likewise displayed only when p < 0.1. Error bars denote ± standard error of the mean; colours denote different populations.

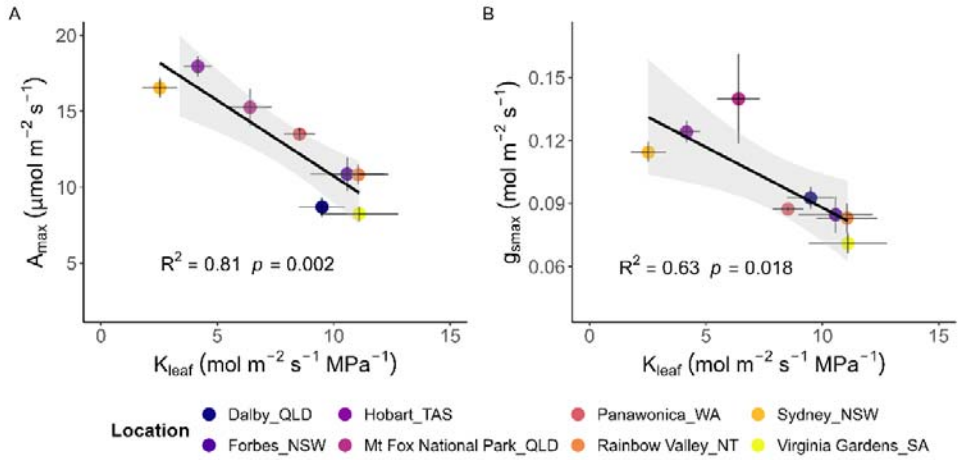

Figure 8: Linear regressions examining the relationships between leaf hydraulic conductance and leaf gas exchange across populations of *T. triandra*. Correlations between leaf hydraulic conductance (K_{leaf}) and (A) maximum photosynthetic rate (A_{max}) and (B) maximum stomatal conductance (g_{smax}). Solid lines and shaded 95% confidence bands are displayed only for statistically significant relationships (P < 0.1). Adjusted R^2 values and P-values (derived from Pearson correlations, equivalent to simple OLS tests) are likewise displayed only when p < 0.1. Error bars denote ± standard error of the mean; colours denote different populations.

REFERENCES

Baird AS, Taylor SH, Pasquet-Kok J, Vuong C, Zhang Y, Watcharamongkol T, Cochard H, Scoffoni C, Edwards EJ, Osborne CP, *et al.* 2025. Resolving the contrasting leaf hydraulic adaptation of C_3 and C_4 grasses. *New Phytologist* 245: 1924–1939.

Balachowski JA, Bristiel PM, Volaire FA. 2016. Summer dormancy, drought survival and functional resource acquisition strategies in California perennial grasses. *Annals of Botany* 118: 357–368.

Bartlett MK, Klein T, Jansen S, Choat B, Sack L. 2016. The correlations and sequence of plant stomatal, hydraulic, and wilting responses to drought. *Proceedings of the National Academy of Sciences* 113: 13098–13103.

Bartlett MK, Scoffoni C, Ardy R, Zhang Y, Sun S, Cao K, Sack L. 2012. Rapid determination of comparative drought tolerance traits: using an osmometer to predict turgor loss point. *Methods in Ecology and Evolution* 3: 880–888.

Bartlett MK, Zhang Y, Kreidler N, Sun S, Ardy R, Cao K, Sack L. 2014. Global analysis of plasticity in turgor loss point, a key drought tolerance trait (J Gurevitch, Ed.). *Ecology Letters* 17: 1580–1590.

Bayramzadeh V, Attarod P, Ahmadi MT, Rezaee Amruabadi SH, Kubo T. 2011. Does the climate of the origin control anatomical characteristics of the vessel elements as well as different foliar traits in Fagus crenata? *Journal of Forest Science* 57: 377–383.

Bjorkman AD, Myers-Smith IH, Elmendorf SC, Normand S, Rüger N, Beck PSA, Blach-Overgaard A, Blok D, Cornelissen JHC, Forbes BC, *et al.* 2018. Plant functional trait change across a warming tundra biome. *Nature* 562: 57–62.

Blackman CJ. 2018. Leaf turgor loss as a predictor of plant drought response strategies. *Tree Physiology* 38: 655–657.

Blackman CJ, Aspinwall MJ, Tissue DT, Rymer PD. 2017. Genetic adaptation and phenotypic plasticity contribute to greater leaf hydraulic tolerance in response to drought in warmer climates. *Tree Physiology* 37: 583–592.

Blackman CJ, Gleason SM, Chang Y, Cook AM, Laws C, Westoby M. 2014. Leaf hydraulic vulnerability to drought is linked to site water availability across a broad range of species and climates. *Annals of Botany* 114: 435–440.

Blackman CJ, Halliwell B, Hartill GE, Brodribb TJ. 2024. Petiole XLA (xylem to leaf area ratio) integrates hydraulic safety and efficiency across a diverse group of eucalypt leaves. *Plant, Cell & Environment* 47: 49–58.

Blonder BW, Aparecido LMT, Hultine KR, Lombardozzi D, Michaletz ST, Posch BC, Slot M, Winter K. 2023. Plant water use theory should incorporate hypotheses about extreme environments, population ecology, and community ecology. *New Phytologist* 238: 2271–2283.

Bourne AE, Creek D, Peters JMR, Ellsworth DS, Choat B. 2017. Species climate range influences hydraulic and stomatal traits in Eucalyptus species. *Annals of Botany* 120: 123–133.

Brodribb TJ, Feild TS, Jordan GJ. 2007. Leaf Maximum Photosynthetic Rate and Venation Are Linked by Hydraulics. *Plant Physiology* 144: 1890–1898.

Brodribb TJ, Holbrook NM. 2003. Stomatal Closure during Leaf Dehydration, Correlation with Other Leaf Physiological Traits. *Plant Physiology* 132: 2166–2173.

Brodribb TJ, Holbrook NM. 2006. Declining hydraulic efficiency as transpiring leaves desiccate: two types of response*. *Plant, Cell & Environment* 29: 2205–2215.

Brodribb TJ, Jordan GJ. 2008. Internal coordination between hydraulics and stomatal control in leaves. *Plant, Cell & Environment* 31: 1557–1564.

Brodribb TJ, Skelton RP, McAdam SAM, Bienaimé D, Lucani CJ, Marmottant P. 2016. Visual quantification of embolism reveals leaf vulnerability to hydraulic failure. *New Phytologist* 209: 1403–1409.

Chen J-W, Zhang Q, Li X-S, Cao K-F. 2009. Independence of stem and leaf hydraulic traits in six Euphorbiaceae tree species with contrasting leaf phenology. *Planta* 230: 459–468.

Choat B, Brodribb TJ, Brodersen CR, Duursma RA, López R, Medlyn BE. 2018. Triggers of tree mortality under drought. *Nature* 558: 531–539.

Choat B, Jansen S, Brodribb TJ, Cochard H, Delzon S, Bhaskar R, Bucci SJ, Feild TS, Gleason SM, Hacke UG, *et al.* 2012. Global convergence in the vulnerability of forests to drought. *Nature* 491: 752–755.

Churchill AC, Zhang H, Fuller KJ, Amiji B, Anderson IC, Barton CVM, Carrillo Y, Catunda KLM, Chandregowda MH, Igwenagu C, *et al.* 2022. Pastures and Climate Extremes: Impacts of Cool Season Warming and Drought on the Productivity of Key Pasture Species in a Field Experiment. *Frontiers in Plant Science* 13: 836968.

Corso D, Delzon S, Lamarque LJ, Cochard H, Torres-Ruiz JM, King A, Brodribb T. 2020. Neither xylem collapse, cavitation, or changing leaf conductance drive stomatal closure in wheat. *Plant, Cell & Environment* 43: 854–865.

Craine JM, Ocheltree TW, Nippert JB, Towne EG, Skibbe AM, Kembel SW, Fargione JE. 2013. Global diversity of drought tolerance and grassland climate-change resilience. *Nature Climate Change* 3: 63–67.

Davis SD, Sperry JS, Hacke UG. 1999. The relationship between xylem conduit diameter and cavitation caused by freezing. *American Journal of Botany* 86: 1367–1372.

Dunning LT, Liabot A-L, Olofsson JK, Smith EK, Vorontsova MS, Besnard G, Simpson KJ, Lundgren MR, Addicott E, Gallagher RV, *et al.* 2017. The recent and rapid spread of *Themeda triandra*. *Botany Letters* 164: 327–337.

Fontes CG, Pinto-Ledezma J, Jacobsen AL, Pratt RB, Cavender-Bares J. 2022. Adaptive variation among oaks in wood anatomical properties is shaped by climate of origin and shows limited plasticity across environments. *Functional Ecology* 36: 326–340.

Franks PJ. 2006. Higher rates of leaf gas exchange are associated with higher leaf hydrodynamic pressure gradients. *Plant, Cell & Environment* 29: 584–592.

Fravolini A. 2002. Carbon isotope discrimination and bundle sheath leakiness in three C4 subtypes grown under variable nitrogen, water and atmospheric CO2 supply. *Journal of Experimental Botany* 53: 2261–2269.

Gleason SM, Westoby M, Jansen S, Choat B, Hacke UG, Pratt RB, Bhaskar R, Brodribb TJ, Bucci SJ, Cao K-F, *et al.* 2016. Weak tradeoff between xylem safety and xylem-specific hydraulic efficiency across the world's woody plant species. *New Phytologist* 209: 123–136.

Guan X, Wen Y, Zhang Y, Chen Z, Cao K-F. 2023. Stem hydraulic conductivity and embolism resistance of *Quercus* species are associated with their climatic niche (J Martinez-Vilalta, Ed.). *Tree Physiology* 43: 234–247.

Hacke UG, Sperry JS, Wheeler JK, Castro L. 2006. Scaling of angiosperm xylem structure with safety and efficiency. *Tree Physiology* 26: 689–701.

Hao G-Y, Lucero ME, Sanderson SC, Zacharias EH, Holbrook NM. 2013. Polyploidy enhances the occupation of heterogeneous environments through hydraulic related trade-offs in Atriplex canescens (Chenopodiaceae). *New Phytologist* 197: 970–978.

Hartill GE, Blackman CJ, Halliwell B, Jones RC, Holland BR, Brodribb TJ. 2023. Cold temperature and aridity shape the evolution of drought tolerance traits in Tasmanian species of Eucalyptus. *Tree Physiology* 43: 1493–1500.

Hartmann H, Link RM, Schuldt B. 2021. A whole-plant perspective of isohydry: stem-level support for leaf-level plant water regulation (S Sevanto, Ed.). *Tree Physiology* 41: 901–905.

Hochberg U, Rockwell FE, Holbrook NM, Cochard H. 2018. Iso/Anisohydry: A Plant–Environment Interaction Rather Than a Simple Hydraulic Trait. *Trends in Plant Science* 23: 112–120.

Hoover DL, Knapp AK, Smith MD. 2014. Resistance and resilience of a grassland ecosystem to climate extremes. *Ecology* 95: 2646–2656.

Huang R, Di N, Xi B, Yang J, Duan J, Li X, Feng J, Choat B, Tissue D. 2024. Herb hydraulics: Variation and correlation for traits governing drought tolerance and efficiency of water transport. *Science of The Total Environment* 907: 168095.

Huxman TE, Winkler DE, Mooney KA. 2022. A common garden super-experiment: An impossible dream to inspire possible synthesis. *Journal of Ecology* 110: 997–1004.

Jacob V, Choat B, Churchill AC, Zhang H, Barton CVM, Krishnananthaselvan A, Post AK, Power SA, Medlyn BE, Tissue DT. 2022. High safety margins to drought-induced hydraulic failure found in five pasture grasses. *Plant, Cell & Environment* 45: 1631–1646.

Jankowski A, Wyka TP, Żytkowiak R, Danusevičius D, Oleksyn J. 2019. Does climate-related in situ variability of Scots pine (Pinus sylvestris L.) needles have a genetic basis? Evidence from common garden experiments. *Tree Physiology* 39: 573–589.

Jardine EC, Thomas GH, Osborne CP. 2021. Traits explain sorting of C_4 grasses along a global precipitation gradient. *Ecology and Evolution* 11: 2669–2680.

Johnson KM, Jordan GJ, Brodribb TJ. 2018. Wheat leaves embolized by water stress do not recover function upon rewatering. *Plant Cell and Environment* 41: 2704–2714.

Karger DN, Conrad O, Böhner J, Kawohl T, Kreft H, Soria-Auza RW, Zimmermann NE, Linder HP, Kessler M. 2017. Climatologies at high resolution for the earth's land surface areas. *Scientific Data* 4: 170122.

Keep T, Sampoux J, Barre P, Blanco-Pastor J, Dehmer KJ, Durand J, Hegarty M, Ledauphin T, Muylle H, Roldán-Ruiz I, *et al.* 2021. To grow or survive: Which are the strategies of a perennial grass to face severe seasonal stress? (K McCulloh, Ed.). *Functional Ecology* 35: 1145–1158.

Lamy J-B, Delzon S, Bouche PS, Alia R, Vendramin GG, Cochard H, Plomion C. 2014. Limited genetic variability and phenotypic plasticity detected for cavitation resistance in a Mediterranean pine. *New Phytologist* 201: 874–886.

Larter M, Pfautsch S, Domec J, Trueba S, Nagalingum N, Delzon S. 2017. Aridity drove the evolution of extreme embolism resistance and the radiation of conifer genus *Callitris*. *New Phytologist* 215: 97–112.

Lens F, Picon-Cochard C, Delmas CE, Signarbieux C, Buttler A, Cochard H, Jansen S, Chauvin T, Chacon Doria L, Del Arco M, *et al.* 2016. Herbaceous angiosperms are not more vulnerable to drought-induced embolism than angiosperm trees. *Plant Physiology*: pp.00829.2016.

Li X, Blackman CJ, Choat B, Duursma RA, Rymer PD, Medlyn BE, Tissue DT. 2018. Tree hydraulic traits are coordinated and strongly linked to climate-of-origin across a rainfall gradient. *Plant, Cell & Environment* 41: 646–660.

Li S, Lens F, Espino S, Karimi Z, Klepsch M, Schenk HJ, Schmitt M, Schuldt B, Jansen S. 2016. INTERVESSEL PIT MEMBRANE THICKNESS AS A KEY DETERMINANT OF EMBOLISM RESISTANCE IN ANGIOSPERM XYLEM. *IAWA Journal* 37: 152–171.

López R, Cano FJ, Choat B, Cochard H, Gil L. 2016. Plasticity in Vulnerability to Cavitation of Pinus canariensis Occurs Only at the Driest End of an Aridity Gradient. *Frontiers in Plant Science* 7.

López R, Cano FJ, Martin-StPaul NK, Cochard H, Choat B. 2021. Coordination of stem and leaf traits define different strategies to regulate water loss and tolerance ranges to aridity. *New Phytologist* 230: 497–509.

Martínez-Vilalta J, Cochard H, Mencuccini M, Sterck F, Herrero A, Korhonen JFJ, Llorens P, Nikinmaa E, Nolè A, Poyatos R, *et al.* 2009. Hydraulic adjustment of Scots pine across Europe. *New Phytologist* 184: 353–364.

McSteen P, Kellogg EA. 2022. Molecular, cellular, and developmental foundations of grass diversity. *Science*.

Mitchell PJ, O'Grady AP. 2015. Adaptation of Leaf Water Relations to Climatic and Habitat Water Availability. *Forests* 6: 2281–2295.

Mitchell PJ, O'Grady AP, Tissue DT, Worledge D, Pinkard EA. 2014. Co-ordination of growth, gas exchange and hydraulics define the carbon safety margin in tree species with contrasting drought strategies. *Tree Physiology* 34: 443–458.

Morris H, Gillingham MAF, Plavcová L, Gleason SM, Olson ME, Coomes DA, Fichtler E, Klepsch MM, Martínez-Cabrera HI, McGlinn DJ, *et al.* 2018. Vessel diameter is related to amount and spatial arrangement of axial parenchyma in woody angiosperms. *Plant, Cell & Environment* 41: 245–260.

Nardini A, Luglio J. 2014. Leaf hydraulic capacity and drought vulnerability: possible trade-offs and correlations with climate across three major biomes. *Functional Ecology* 28: 810–818.

Nardini A, Salleo S. 2000. Limitation of stomatal conductance by hydraulic traits: sensing or preventing xylem cavitation? *Trees* 15: 14–24.

Ocheltree TW, Nippert JB, Prasad PVV. 2016. A safety vs efficiency trade-off identified in the hydraulic pathway of grass leaves is decoupled from photosynthesis, stomatal conductance and precipitation. *New Phytologist* 210: 97–107.

Olson ME, Soriano D, Rosell JA, Anfodillo T, Donoghue MJ, Edwards EJ, León-Gómez C, Dawson T, Camarero Martínez JJ, Castorena M, *et al.* 2018. Plant height and hydraulic vulnerability to drought and cold. *Proceedings of the National Academy of Sciences* 115: 7551–7556.

Osborne CP, Sack L. 2012. Evolution of C4 plants: a new hypothesis for an interaction of CO2 and water relations mediated by plant hydraulics. *Philosophical Transactions of the Royal Society B: Biological Sciences* 367: 583–600.

Pathare VS, Sonawane BV, Koteyeva N, Cousins AB. 2020. C_4 grasses adapted to low precipitation habitats show traits related to greater mesophyll conductance and lower leaf hydraulic conductance. *Plant, Cell & Environment* 43: 1897–1910.

Peters JMR, López R, Nolf M, Hutley LB, Wardlaw T, Cernusak LA, Choat B. 2021. Living on the edge: A continental-scale assessment of forest vulnerability to drought. *Global Change Biology* 27: 3620–3641.

Pittermann J, Sperry JS. 2006. Analysis of Freeze-Thaw Embolism in Conifers. The Interaction between Cavitation Pressure and Tracheid Size. *Plant Physiology* 140: 374–382.

Schwinning S, Lortie CJ, Esque TC, DeFalco LA. 2022. What common-garden experiments tell us about climate responses in plants. *Journal of Ecology* 110: 986–996.

Scoffoni C, Albuquerque C, Buckley TN, Sack L. 2023. The dynamic multi-functionality of leaf water transport outside the xylem. *New Phytologist* 239: 2099–2107.

Scoffoni C, Chatelet DS, Pasquet-kok J, Rawls M, Donoghue MJ, Edwards EJ, Sack L. 2016. Hydraulic basis for the evolution of photosynthetic productivity. *Nature Plants* 2: 16072.

Skelton RP, Brodribb TJ, McAdam SAM, Mitchell PJ. 2017. Gas exchange recovery following natural drought is rapid unless limited by loss of leaf hydraulic conductance: evidence from an evergreen woodland. *New Phytologist* 215: 1399–1412.

Skelton RP, West AG, Dawson TE. 2015. Predicting plant vulnerability to drought in biodiverse regions using functional traits. *Proceedings of the National Academy of Sciences* 112: 5744–5749.

Snyman HA, Ingram LJ, Kirkman KP. 2013. *Themeda triandra*: a keystone grass species. *African Journal of Range & Forage Science* 30: 99–125.

Sperry JS, Hacke UG, Pittermann J. 2006. Size and function in conifer tracheids and angiosperm vessels. *American Journal of Botany* 93: 1490–1500.

Taylor SH, Ripley BS, Woodward FI, Osborne CP. 2011. Drought limitation of photosynthesis differs between C_3 and C_4 grass species in a comparative experiment. *Plant, Cell & Environment* 34: 65–75.

767 Trueba S, Pouteau R, Lens F, Feild TS, Isnard S, Olson ME, Delzon S. 2017. Vulnerability to xylem
768 embolism as a major correlate of the environmental distribution of rain forest species on a tropical
769 island. *Plant, Cell & Environment* 40: 277–289.

770 Tyree MT, Davis SD, Cochard H. 1994. Biophysical Perspectives of Xylem Evolution: is there a
771 Tradeoff of Hydraulic Efficiency for Vulnerability to Dysfunction? *IAWA Journal* 15: 335–360.

772 VanderWeide BL, Hartnett DC, Carter DL. 2014. Belowground bud banks of tallgrass prairie are
773 insensitive to multi-year, growing-season drought. *Ecosphere* 5: art103.

774 Volaire F, Lens F, Cochard H, Xu H, Chacon-Doria L, Bristiel P, Balachowski J, Rowe N, Violle C, Picon-
775 Cochard C. 2018. Embolism and mechanical resistances play a key role in dehydration tolerance of a
776 perennial grass Dactylis glomerata L. *Annals of Botany* 122: 325–336.

777 Volaire F, Seddaiu G, Ledda L, Lelievre F. 2009. Water deficit and induction of summer dormancy in
778 perennial Mediterranean grasses. *Annals of Botany* 103: 1337–1346.

779 Xiong D, Douthe C, Flexas J. 2018. Differential coordination of stomatal conductance, mesophyll
780 conductance, and leaf hydraulic conductance in response to changing light across species. *Plant, Cell*
781 *& Environment* 41: 436–450.

782 Yao G, Nie Z, Turner NC, Li F, Gao T, Fang X, Scoffoni C. 2021. Combined high leaf hydraulic safety
783 and efficiency provides drought tolerance in *Caragana* species adapted to low mean annual
784 precipitation. *New Phytologist* 229: 230–244.

785 Zanne AE, Westoby M, Falster DS, Ackerly DD, Loarie SR, Arnold SEJ, Coomes DA. 2010. Angiosperm
786 wood structure: Global patterns in vessel anatomy and their relation to wood density and potential
787 conductivity. *American Journal of Botany* 97: 207–215.

788 Zhou H, Akçay E, Edwards E, Helliker B. 2020. The legacy of C_4 evolution in the hydraulics of C_3 and C_4
789 grasses.

790 Zwicke M, Picon-Cochard C, Morvan-Bertrand A, Prud'homme M-P, Volaire F. 2015. What functional
791 strategies drive drought survival and recovery of perennial species from upland grassland? *Annals of*
792 *Botany* 116: 1001–1015.

793

794